

Epitaxial stabilization of ultra thin films of electron doped manganites

S. Middey,^{1,*} M. Kareev,¹ D. Meyers,¹ X. Liu,¹ Y. Cao,¹ S. Tripathi,¹ P. Ryan,² J. W. Freeland,² and J. Chakhalian¹

¹*Department of Physics, University of Arkansas, Fayetteville, Arkansas 72701, USA*

²*Advanced Photon Source, Argonne National Laboratory, Argonne, Illinois 60439, USA*

Ultra-thin films of the electron doped manganite $\text{La}_{0.8}\text{Ce}_{0.2}\text{MnO}_3$ were grown in a layer-by-layer growth mode on SrTiO_3 (001) substrates by pulsed laser interval deposition. High structural quality and surface morphology was confirmed by a combination of synchrotron based x-ray diffraction and atomic force microscopy. Resonant X-ray absorption spectroscopy measurements confirm the presence of Ce^{+4} and Mn^{+2} ions. In addition, the electron doping signature was corroborated by Hall effect measurements. All grown films show ferromagnetic ground state as revealed by both XMCD and magnetoresistance measurements and remain insulating contrary to earlier reports of metal-insulator transition. Our results hint at the possibility of electron-hole asymmetry in the colossal magnetoresistive (CMR) manganite phase diagram akin to high- T_c cuprates.

Hole-doped manganites ($R_{1-x}A_x\text{MnO}_3$) have been extensively studied over the last few decades¹⁻³ not only for the realization of different exotic phenomena (*e.g.* colossal magnetoresistance, phase separation, charge ordering etc.) driven by the strong coupling among the lattice, spin, charge, and orbitals degrees of freedom but also for the huge technological potential of using these materials in spintronic devices⁴⁻⁶. While the hole doping (*i.e.* increase in Mn oxidation state) can be realized by the partial substitution of R^{+3} ions of $\text{RMn}^{+3}\text{O}_3$ by some A^{+2} ions, the successful replacement of R^{+3} by some A^{+4} cations should reduce the same amount of Mn to +2 charge state. The electron doping may result in an asymmetric phase diagram, as for instance has been established for the case of high T_c cuprate family⁷⁻⁹. However, unlike the hole doping in cuprates, where the holes are known to reside on the ligand (oxygen) p orbitals¹⁰, the electrons can be directly doped into the Cu d orbital states¹¹ resulting in a very distinct phase diagram with doping concentration. Towards this end, though the synthesis of the electron doped manganites was expected to be similar to that of the electron-doped cuprates¹² using Ce as dopant, the experimental reports¹³⁻²³ featuring Ce doped LaMnO_3 , are in sharp conflict with each other questioning the feasibility of reliable electron doping for the manganite compounds to investigate this fundamental issue.

Specifically, after the first report of synthesizing Ce doped RMnO_3 ($R = \text{La, Pr, Nd}$) in polycrystalline powder form¹³, the phase diagram of $\text{La}_{1-x}\text{Ce}_x\text{MnO}_3$ thin film was studied as a function of x ¹⁵. It is interesting to note that, contrary to the highly asymmetric $T-x$ phase diagram of high T_c cuprates family⁸, the phase diagram of manganites (LaR) MnO_3 as a function of hole²⁴ and electron doping¹⁵ appeared to be surprisingly symmetric. While the electron doping in $\text{La}_{0.7}\text{Ce}_{0.3}\text{MnO}_3$ was conjectured from the observation of Ce^{+4} valency in the XAS spectrum¹⁶ and from experiments with a $p-n$ junction composed of hole and electron doped manganites layers^{17,18}, the latter reports^{22,23} have argued that the ferromagnetism and insulator to metal transition (IMT) may arise from uncontrolled *hole* doping. In addition, the Hall effect measurements on $\text{La}_{0.7}\text{Ce}_x\text{MnO}_{3+\delta}$ with varying oxygen content δ demonstrated²¹ that the samples with electrons as the carrier type lack any IMT and remain insulating throughout the whole temperature range. Those contradicting reports have intensified the overall concern about the true nature of electronic and magnetic ground state in electron doped manganites generated by the Ce doping.

In this letter, we have report on the growth of high quality thin films of $\text{La}_{0.8}\text{Ce}_{0.2}\text{MnO}_3$ on a SrTiO_3 (001) substrate using pulsed laser interval deposition technique. While the extensive structural and surface morphology characterization using reflection high energy electron diffraction (RHEED), atomic force microscopy (AFM), synchrotron based X-ray diffraction (XRD) confirmed excellent structural quality of the films; the presence of electron doping was confirmed by resonant X-ray absorption spectroscopy on Mn $L_{3,2}$ and Ce $M_{4,5}$ -edge and by Hall effect measurements. The presence of ferromagnetism was assessed by XMCD on Mn L-edge and by magnetoresistance measurements up to 7T. Contrary to the earlier reports of metal-insulator transition for this composition, our electron doped samples remain insulating throughout the whole temperature range of measurement with ferromagnetic ground state.

$\text{La}_{0.8}\text{Ce}_{0.2}\text{MnO}_3$ films with 20 uc (unit cell) thickness were grown on high-quality SrTiO_3 (STO) (001) substrates (Crystec, Germany) by pulsed laser interval deposition²⁵ using a KrF excimer laser operating at $\lambda = 248$ nm and 18 Hz pulse rate. The growth was carried out at 870°C under 250 mTorr partial pressure of oxygen and the entire layer by layer growth process was monitored in-situ by high pressure RHEED. In order to avoid the over oxidation of the samples by annealing at the growth temperature, the sample was first cooled down to 600°C at a rate of 15°C/min immediately after finishing the growth and then annealed for 30 minutes under 500 Torr of ultra pure oxygen. The X-ray diffraction patterns were recorded at the 6-ID-B beam line of the Advanced Photon Source (APS). In order to determine charge state of Mn and Ce, resonant X-ray absorption spectra of Mn $L_{3,2}$ edge and Ce $M_{4,5}$ edges have been acquired at the 4-ID-C beam line of the APS in total electron yield (TEY) mode. The thickness (~ 7.8 nm) of these films compared to the probing depth (~ 10 nm) of the TEY mode allow us to probe the electronic and magnetic structure throughout the entire sample. The magneto-transport properties and Hall resistance in an applied magnetic field up to 7 T were measured in a Physical Property Measurement system (PPMS).

The time dependent intensity of the specular reflection of the RHEED pattern during growth are shown in Fig. 1(a). As seen, the intensity sharply drops during the rapid ablation and recovers within the next few seconds, confirming the layer-by-layer growth.^{25,26} The characteristic specular (0,0) and off-specular reflection (0,1) & (0,-1) Bragg reflections together with the streaking patterns in the diffraction image (Fig. 1(b)) obtained after cooling to room temperature imply smooth flat terraces. The absence of any half-order peaks²⁶ in the RHEED patterns implies that any orthorhombic distortion, if present, must be very small. The AFM image of the surface morphology of the film is shown in Fig. 1(c) yields an average surface roughness ~ 95 pm, further affirming their high morphological quality. Additionally, the structural quality of the grown film has been investigated by synchrotron based x-ray diffraction. Fig. 1(d) displays the diffraction pattern obtained in the vicinity of the STO (0 0 1) reflection. As seen, the broad film peak, marked by the arrow corresponds to the out-of-plane lattice constant of 3.8663 Å; the result is consistent with the expected tetragonal distortion under tensile strain for the cube on cube growth.

After confirming the high structural quality of the samples, we turn our attention to the key question of electron doping. As Ce can have both +3 and +4 oxidation states, the key criterion of electron doping is the presence of stabilized Ce^{+4} in our film. To this end we used resonant X-ray absorption which is a direct probe of the charge

oxidation state²⁷. Fig. 2(a) shows the XAS pattern obtained at the Ce $M_{4,5}$ edge along with the reference spectra reported earlier from Ce(+4)O₂ and Ce(+3)F₃ standards¹⁶. A direct comparison to the Ce reference samples reveals that the LCeMO line shape is very similar to that of Ce(+4)O₂ standard. At the same time the LCeMO spectrum has additional small features at the lower energy side for both M_5 and M_4 edges. Specifically, the additional low intensity shoulder around 886 eV matches the main peak of M_5 edge for Ce(+3)F₃ implying the small contribution of Ce in the +3 oxidation state. This implies that the magnitude of the electron doping concentration is slightly lower than nominal 20% doping expected from the formal chemical formulae. Complimentary to Ce XAS results, Fig. 2(b) shows the Mn L_3 edge XAS spectra for the LCeMO film and Mn(+2)O standard recorded simultaneously with the sample in the diagnostic section of the beamline. As shown, the shoulder position at 638.7 eV matches exactly with the position of the main peak of the MnO standard and thus clearly indicates the presence of *divalent* Mn within the electron doped LCeMO film. In short, the combined presence of Ce⁺⁴ and Mn⁺² charge states directly establishes the formation of the electron doped phase of LCeMO.

With the knowledge of electronic structure we precede with studies of magnetization and magneto-transport properties of the LCeMO. Towards this end, the temperature-dependent resistivity behaviors, with and without external magnetic field were measured during cooling and heating cycles; since both curves are identical only the cooling curves are shown in Fig. 3(a). Contrary to the earlier reports by Zhao *et al.*¹⁹ suggesting that La_{0.8}Ce_{0.2}MnO₃ films would undergo a metal-insulator transition due to hole doping, the present film is insulating at all temperatures and does not show any transition to the metallic state. To exclude the effect of strain we have grown 20 uc LCeMO film on YAlO₃ under large compressive strain. The resulting sample is still insulating at the whole temperature range (not shown) thus affirming the robustness of the insulating ground state. The application of an external magnetic field results in large negative magnetoresistance (see Fig. 3(a) and inset), characteristic of colossal magnetoresistance. In order to define the carrier type (hole vs. electron), the Hall effect has been measured by sweeping the magnetic field (H) between -7 T and +7 T at different temperatures. Figure 3(b) shows the dependence of transverse Hall resistivity (ρ_{xy})²⁸ on H . As observed, the negative sign of R_H at 200 K highlights the excellent agreement with our conclusion on electron doping obtained from XAS measurements. As a rough estimate, assuming a Fermi surface with one type of charge carriers, the carrier concentration n ($R_H=1/ne$) can be estimated $\sim 3.6 \times 10^{20}$ electrons/cm³. In passing we note, our Hall resistance results are in variance with the earlier reports^{21,23} about positive Hall coefficient in Ce doped manganite. In order to further confirm the presence of ferromagnetism, x-ray absorption spectra at the Mn $L_{3,2}$ edges were recorded with left and right circularly polarized light. The strong XMCD (x-ray magnetic circular dichroism) signal (Fig. 3(c)) obtained at 150 K with an applied 5 Tesla magnetic field establishes the characteristic ferromagnetic response of Mn in this electron doped sample.

In summary, we have developed the layer-by-layer growth of high quality fully epitaxial films of electron doped LCeMO manganites. A combination of RHEED, synchrotron based XRD and XAS confirmed the excellent structural, chemical, and electronic quality, while transport measurements confirmed the insulating nature of the film. The presence of ferromagnetism is determined from the large magnetoresistance and Mn XMCD signal. The Hall effect measurements corroborates that electron as the charge carrier. The present study hints at the possible electron-hole asymmetry in the CMR manganite phase diagram and opens exciting possibilities of merging this electron doped material with the other hole doped systems to fabricate oxide based spintronic junctions.

J. C. was supported by DOD-ARO under Grant No. 0402-17291. Work at the Advanced Photon Source, Argonne was supported by the U.S. Department of Energy, Office of Science under Grant No. DEAC02-06CH11357.

* smiddey@uark.edu

¹ E. Dagotto, T. Hotta, and A. Moreo, Physics Reports **344**, 1 (2001).

² M. B. Salamon, and M. Jaime, Rev. Mod. Phys. **73**, 583 (2001).

³ Y. Tokura, Rep. Prog. Phys. **69** 797 (2006).

⁴ A-M Haghir-Gosnet, and J-P Renard J. Phys. D: Appl. Phys. **36**, R127 (2003).

⁵ C. H. Ahn, A. Bhattacharya, M. Di Ventura, J. N. Eckstein, C. Daniel Frisbie, M. E. Gershenson, A. M. Goldman, I. H. Inoue, J. Mannhart, A. J. Millis, A. F. Morpurgo, D. Natelson, and J.-M. Triscone, Rev. Mod. Phys. **78**, 1185 (2006).

⁶ T. Yajima, Y. Hikita, and H. Y. Hwang, Nature Matter. **10**, 198 (2011).

⁷ C. Weber, K. Haule, and G. Kotliar, Nature Physics **6**, 574 (2010).

⁸ D. N. Basov, and A. V. Chubukov, Nature Physics **7**, 272 (2011).

⁹ N. P. Armitage, P. Fournier, and R. L. Greene, Rev. Mod. Phys. **82**, 2421 (2010).

¹⁰ N. Nücker, J. Fink, J. C. Fuggle, P. J. Durham, and W. M. Temmerman, Phys. Rev. B **37**, 5158 (1988).

¹¹ G. Liang, Y. Guo, D. Badresingh, W. Xu, Y. Tang, M. Croft, J. Chen, A. Sahiner, Beom-hoan O and J. T. Markert, Phys. Rev. B, **51**, 1258 (1995).

¹² Y. Tokura, H. Takagi, and S. Uchida, Nature **337**, 345 (1989).

¹³ P. Mandal and S. Das, Phys. Rev. B **56**, 15073 (1997).

- ¹⁴ C. Mitra, P. Raychaudhuri, J. John, S. K. Dhar, A. K. Nigam, and R. Pinto, J. Appl. Phys. **89**, 524 (2001).
- ¹⁵ P. Raychaudhuri, C. Mitra, P. D. A. Mann, and S. Wirth, J. Appl. Phys. **93**, 8328 (2003).
- ¹⁶ C. Mitra, Z. Hu, P. Raychaudhuri, S. Wirth, S. I. Csiszar, H. H. Hsieh, H.-J. Lin, C. T. Chen, and L. H. Tjeng, Phys. Rev. B **67**, 092404 (2003).
- ¹⁷ C. Mitra, P. Raychaudhuri, G. Köbernik, K. Dörr, K. -H. Müller, L. Schultz, and R. Pinto, Appl. Phys. Lett., **79**, 2408 (2001).
- ¹⁸ C. Mitra, P. Raychaudhuri, Dörr, K. -H. Müller, L. Schultz, P.M. Oppeneer, and S.Wirtt, Phys. Rev. Lett., **90**, 017202 (2003).
- ¹⁹ Y.G. Zhao, R.C. Srivastava, P. Fournier, V. Smolyaninova, M. Rajeswari, T. Wu, Z.Y. Li, R.L. Greene, and T. Venkatesan, J. Magn. & Magn. Mater. **220**, 161 (2000).
- ²⁰ T. Yanagida, T. Kanki, B. Vilquin, H. Tanaka, and T. Kawai, Phys. Rev. B **70**, 184437 (2004).
- ²¹ D. J. Wang, J. R. Sun, S. Y. Zhang, G. J. Liu, and B. G. Shen, H. F. Tian and J. Q. Li, Phys. Rev. B **73**, 144403 (2006).
- ²² T. Yanagida, Y. Saitoh, Y. Takeda, A. Fujimori, H. Tanaka, and T. Kawai, Phys. Rev. B **79**, 132405 (2009).
- ²³ R. Werner, C. Raisch, V. Leca, V. Ion, S. Bals, G. Van Tendeloo, T. Chasse, R. Kleiner, and D. Koelle, Phys. Rev. B **79**, 054416 (2009).
- ²⁴ P. Schiffer, A. P. Ramirez, W. Bao, and S.-W. Cheong, Phys. Rev. Lett. **75**, 3336 (1995).
- ²⁵ M. Kareev, *et al.* J. Appl. Phys. **109**, 114303 (2011).
- ²⁶ D. Meyers, *et al.* J. Phys. D: Appl. Phys. **46**, 385303 (2013).
- ²⁷ B. T. Thole, G. van der Laan, J. C. Fuggle, G. A. Sawatzky, R. C. Karnatak, and J. M. Esteve, Phys. Rev. B **32**, 5107 (1985).
- ²⁸ Here we recap, that for a ferromagnet, the Hall resistivity²⁹ is given by $\rho_{xy} = \mu_0 [R_s M + R_H H]$ with R_s , R_H being the anomalous and the ordinary Hall coefficients respectively, where μ_0 is the vacuum permeability and M is the magnetization. In order to remove the magnetoresistance contribution which are an even function of H , ρ_{xy} has been obtained from the measured Hall resistivity (ρ_{raw}) as follows $\rho_{xy} = [\rho_{raw}(\uparrow, +) - \rho_{raw}(\downarrow, -)]/2$, where $\downarrow, \uparrow, +, -$ present the increasing, decreasing, positive, negative external H , respectively^{30,31}.
- ²⁹ N. Nagaosa, J. Sinova, S.i Onoda, A. H. MacDonald, and N. P. Ong, Rev. Mod. Phys. **82**, 1539 (2010).
- ³⁰ K. Y. Wang, K. W. Edmonds, L. X. Zhao, M. Sawicki, R. P. Campion, B. L. Gallagher, and C. T. Foxon, Phys. Rev. B **72**, 115207 (2005).
- ³¹ H. S. Hsu, C. P. Lin, H. Chou, and J. C. A. Huang, Appl. Phys. Lett., **93**, 142507 (2008).

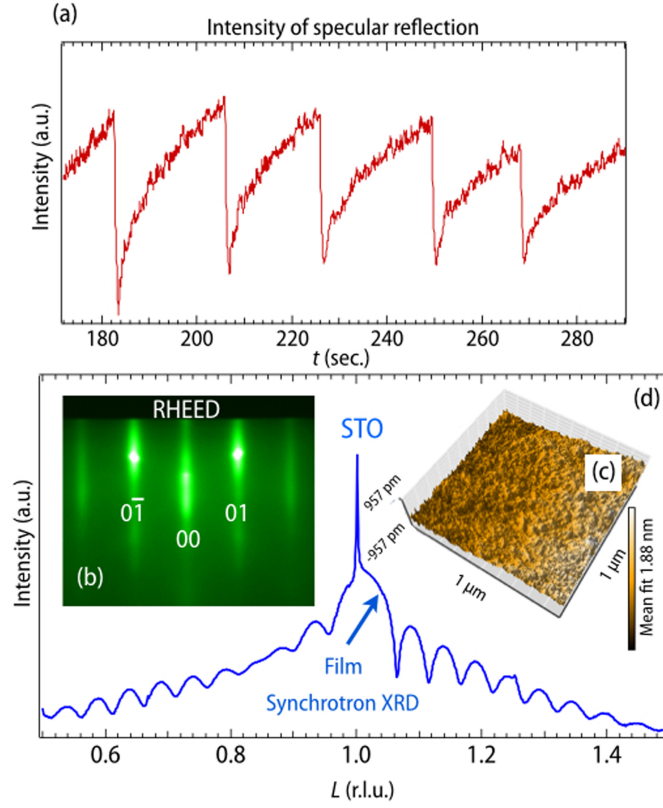


FIG. 1. (Color online) (a) RHEED specular intensity during the growth on STO substrate. (b) RHEED pattern of the 0th Laue circle on the same LCeMO film obtained after cooling to room temperature. The RHEED images were obtained along $[010]$ direction. (c) AFM image (d) XRD pattern around STO (001) reflection.

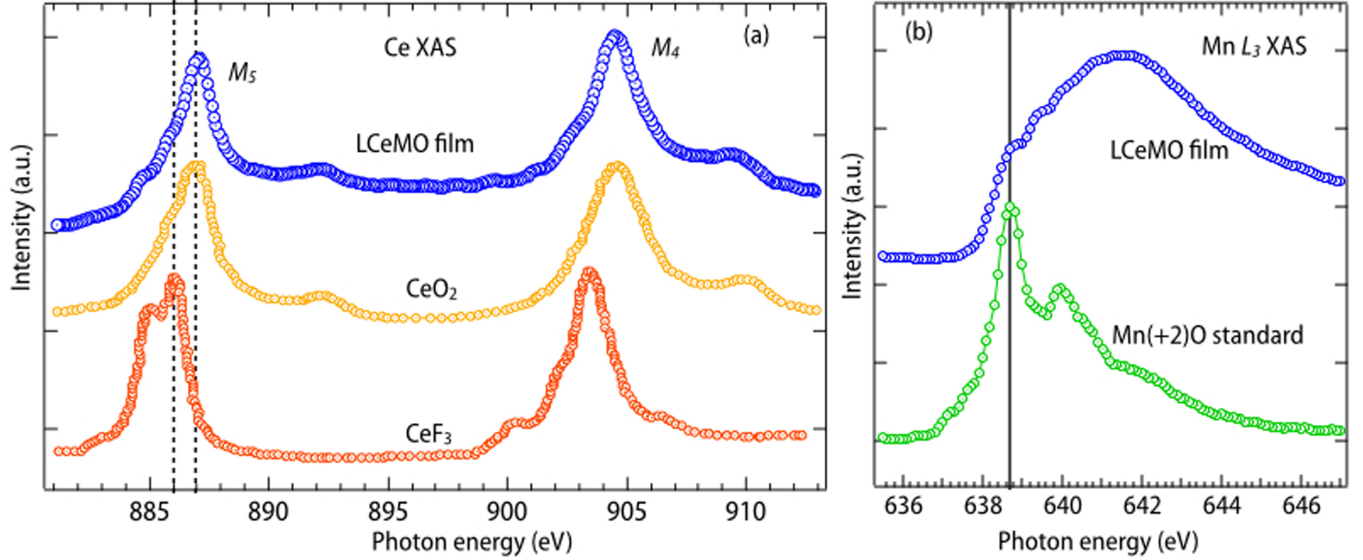


FIG. 2. (Color online) (a) Ce $M_{5,4}$ XAS spectrum of $\text{La}_{0.8}\text{Ce}_{0.2}\text{MnO}_3$ film has been compared with the spectra of CeO_2 and CeF_3 standard, reproduced from Ref. ¹⁶. (b) Mn L_3 XAS spectra of $\text{La}_{0.8}\text{Ce}_{0.2}\text{MnO}_3$ film and $\text{Mn}(+2)\text{O}$ standard. All of the data in both panel (a) and (b) are moved arbitrarily along y axis for visual clarity.

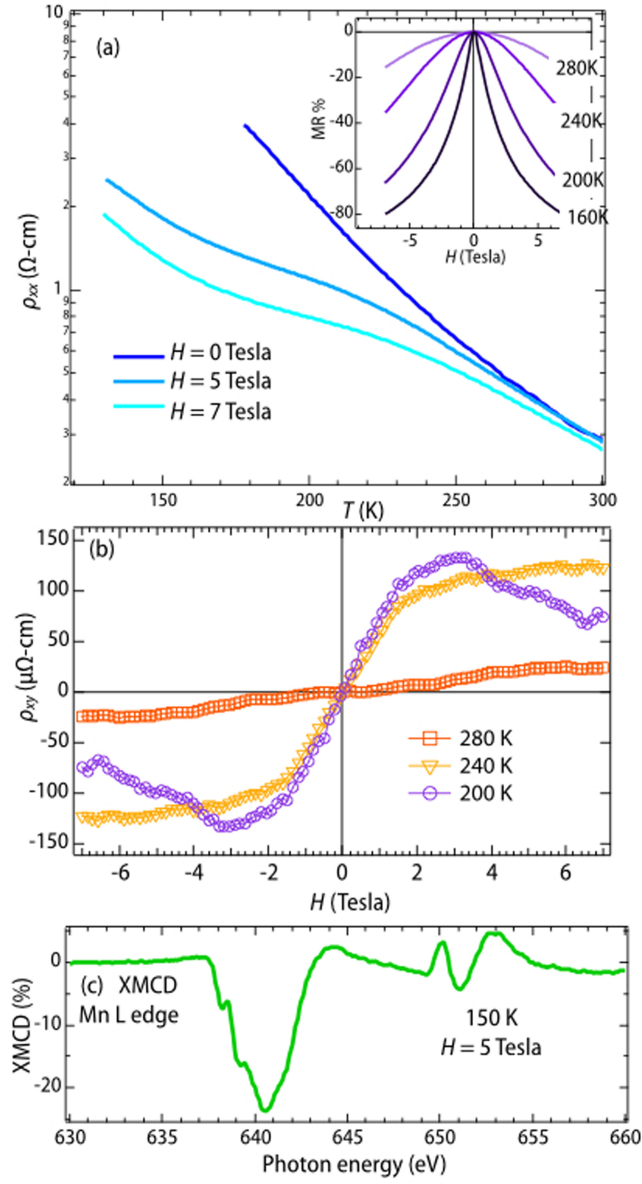


FIG. 3. (Color online) (a) Resistivity vs. temperature for 20 uc LCeMO film measured with different magnetic field. The inset shows magnetoresistance (MR) as a function H at several T . MR is defined as $\text{MR}(H) = \rho_{xx}$ (b) Field dependence of the Hall resistivity measured at different T . (c) XMCD measurements at the Mn $L_{3,2}$ edges.